Eur. Phys. J. B **9**, 343–354 (1999)

**THE EUROPEAN PHYSICAL JOURNAL B**

EDP Sciences


# Minimum description of the onset of pipe turbulence*

U. Brosa and S. Grossmann[a]

Philipps-Universität, Renthof 6, 35032 Marburg, Germany

Received 20 October 1997

**Abstract.** To demonstrate essentials of the mechanism for the onset of turbulence in a pipe at $Re = 2000$, 48 degrees of freedom are enough. The derivation from the Navier-Stokes equation uses a novel type of modes which guarantee linear stability. For the reduction of the nonlinear interactions, the modes are grouped in 3 blocks. Facilitated by these simplifications the interdependence between linear and nonlinear processes is analysed, however, just for a special example. A phenomenon resembling backflow is identified.

**PACS.** 47.27.Cn Transition to turbulence – 47.20.Ft Instability of shear flows – 47.11.+j Computational methods in fluid dynamics

## 1 Introduction: Scrutinizing the clockwork

Various hydrodynamic flows, including Hagen-Poiseuille flow through a pipe, are linearly stable but become turbulent nevertheless. The mechanism which leads to the transition from the laminar to the turbulent flow seems to be a constructive interplay between the *linearly* driven transient growth of disturbances and the *nonlinear* interactions of the sufficiently strengthened deviations from the laminar flow ([1], see also [2] for a recent compilation of references). The energy for the transient growth comes from the mean flow imposed by the external conditions. It is the nonnormality of the linearized flow equations which implies a subdivision of all perceivable disturbances: there is one set of modes, which we call the "providers", which fetch the energy from the mean flow, and there is the complementary set of modes, denoted as the "consumers", which dissipate the energy but determine the features of the turbulent flow. A positive feedback is constituted if these consumers interact to excite new providing modes. In contrast to the exponential growth of small deviations from an unstable flow, the nonnormal-nonlinear interplay leads to an algebraic increase of disturbances but is similarly effective.

This transition mechanism has many still unexplored features. In particular, the details of the nonlinear interactions are unclear yet. Also, the positive feedback loop *cannot* be understood in an *infinitesimal* time step, as it is possible in truely unstable situations via those eigenmodes whose eigenvalues have a positive real part. In the linearly stable but nonnormal situation of pipe flow the providing modes cannot regenerate themselves: nonnormality holds *within* subspaces of modes with fixed azimuthal and axial wave numbers $m$ and $\beta$; these modes cannot interact. Nonlinear interactions on the other hand are possible only for *different* $[m|\beta]$-subspaces, which are orthogonal and thus normal to each other.

To analyse the feedback which leads from laminar to turbulent flow one thus has to integrate the equations of motion over *finite* times. This paper intends to study this by solving the Navier-Stokes equations reduced to a finite space of appropriate modes. It will turn out that for $Re = 2000$ already 48 such modes suffice, if properly chosen, to constitute a successful feedback loop. This dimension is much less than the common eigenmode expansions seem to indicate but much more than in true instability transitions, where just one eigenmode with a positive real part of its eigenvalue is necessary and sufficient.

We concentrate on the cooperation between nonnormality and nonlinearity to feed and to sustain disturbances of the laminar flow, but do not study the phase space structure once the turbulent state has been reached. As it has been reported [3,4] for the case of plane Couette flow, there may also be chaotic repellors or unstable stationary states in Poiseuille pipe flow. This is not considered in the present paper.

Our aim is to contribute to our understanding of the basic mechanism for the onset of turbulence in pipe flow similarly as an old-fashioned watchmaker examines every cogwheel of a clockwork when he intents to repair it. So our method differs from previous work with low-dimensional models: we let the Navier-Stokes equation decide which degrees of freedom it needs rather than indulge ourselves with contrived models.

The notions and numerical details we use are the common ones, see *e.g.* [1]. We shall repeat them here as far as necessary to make the paper selfcontained. A slight change of terminology, however, is necessary. It is induced by facts that we want to explain now. Namely, with growing

* With congratulations to Heinz Horner on the occasion of his 60th birthday.

[a] e-mail: grossmann_s@physik.uni-marburg.de

Reynolds number the linearized Navier-Stokes operator gets increasingly nonnormal, such that its eigenfunctions become more and more parallel and therefore need larger and larger coefficients when they are to represent an arbitrary flow as a series expansion. In a simplified manner one may say that the set of eigenfunctions of the nonnormal linear Navier-Stokes operator spans only a subspace in the space of all flows. In [1] the flow fields that can be represented by series with reasonably small coefficients were called *daughters* while all others became *mothers*. By this definition the daughters are flows which are more or less contained in the space spanned by the eigenfunctions of the linear Navier-Stokes operator while the mothers are in essence perpendicular to that space. The idea was that the mothers are able to provide the energy (which they gain from the mean flow) that the daughters then consume. This, however, turned out to be not entirely correct. It is true that all daughters consume energy, but not all mothers provide it. Energy can be drawn from the basic flow only by such flow disturbing modes which belong to the complement of the eigenspace *and* are not detrimentally damped. It would thus have been better to call the daughters *fit* functions and the mothers *misfits*, to underline their relation to the direction, in which the eigenfunctions bunch, and to state that just a few misfits induce amplification, namely those with small damping.

The two-dimensional models, which were built to make linear amplification despite linear stability comprehensible [1, Sect. 4.2], [2], [5, Sect. 5], [6,7], can lead to a misinterpretation of the fit-misfit mechanism. In these models there exists essentially only one damping constant. In realistic systems with more degrees of freedom multiple damping occurs.

To eschew misunderstandings by using terminologies, which refer only to the geometry of the eigenfunctions and dismiss their eigenvalues (daughters-mothers, fit-misfit), we better discriminate flows as *providers* and *consumers*. To define them we measure the *quality* of a provider by the amplification of the energy of such a disturbance, which develops according to the Navier-Stokes equation linearized about the laminar flow within a *finite time*. We speak of a consumer if the disturbance experiences no amplification at all.

For the analysis of turbulence we will replace the formerly used Stokes modes (*i.e.*, the eigenmodes of the linearized Navier-Stokes operator with no laminar background at all) or the Hagen modes (*i.e.*, the eigenfunctions of the linearization about the Hagen-Poiseuille profile) by a new, equivalent set of functions neatly ordered by their quality. We will have the consumers with the most wasteful dissipation of energy at the left end (lower values of the labels) of this set of modes, whereas the most powerful providers will appear at the right end (higher values of the labels). This is achieved by a reorganization of the Hagen modes and a subsequent orthogonalization. The procedure (the $QR$ decomposition, see later) guarantees the linear stability, which the full Navier-Stokes equation has, for all expansions of its solutions in terms of *any number* of these new modes – see Section 2.

The new functions, denoted as "$q$-modes", ease the interpretation of the linear processes. We will use this to accomplish two aims.

First, the system of differential equations describing pipe turbulence will be reduced to its minimum size: only 24 complex amplitudes turn out to be necessary at $Re = 2000$ (Sects. 3 and 4). Byproducts of these investigations are the ideas of a "powerhouse", *i.e.*, the community of all providers, and of the "consumption" – compare Section 4. These ideas may be helpful to transfer our methods for pipe flow to other, more complicated types of flows.

Second, the separation into providers and consumers in the linear processes facilitates a closer look to the nonlinear mechanisms. Without nonlinearity the energy transfer from the basic flow to the disturbance would happen but once. To allow for long-lasting turbulence the nonlinearity must at times refuel the powerhouse. By way of an example we shall show how this works, with all the details (Sect. 5).

We do not intend to quantitatively compare with full numerical simulations. Such systematic comparison still has to be done, and we hope the present work will open way to do it. Both those large $N$ simulations as well as our small $N$ calculations, which qualitatively reproduce and demonstrate the intricate cooperation between the linear transient amplification due to nonnormality and the nonlinear interactions on a small $N$ mode Galerkin basis, provide approximate solutions to the Navier-Stokes equation. Having this in mind we take liberty to describe our flow fields in conventional terms like *turbulence, double threshold, profile*, etc., being aware that this is not understood quantitatively.

Thus, when using the notion *turbulence* or *turbulent solution* we mean the chaoticity, *i.e.*, the irregular temporal behavior of the solutions but also their qualitative similarity to some observed features of turbulence. One can compare properties derived from our computed approximate solutions with the corresponding measured ones. Three such observable features will be discussed in this paper: (a) the irregular fluctuations of the flow, (b) the double threshold for the onset of turbulence, *i.e.*, the observation that the Reynolds number *as well as* the initial disturbance must exceed certain values, and (c) the flattening of the calculated approximate velocity profile for the pipe flow, *cf.* Section 6. In any case, our aim is qualitative, structural, not quantitative comparison with turbulence.

Of course, we offer a summary in Section 7. An overview on the physics and the mechanism of the onset of shear turbulence is given in reference [16].

## 2 q-modes

Flow through a straight pipe has axial symmetry and is translational invariant. The first property allows for solutions of the linearized Navier-Stokes equation proportional to $e^{im\varphi}$ where $\varphi$ denotes the azimuthal angle and $m$ an integer. The second property permits factors $e^{i\beta z}$, with $z$ as coordinate along the pipe's axis and $\beta$ as a real wave number.

Hence one may collect all modes in blocks, which are distinguished by their $[m|\beta]$ values. *Linear* interaction, *i.e.*, the coupling of the disturbance to the basic Hagen-Poiseuille flow, mixes the modes only within the blocks, whereas for *nonlinear* interactions as defined by the Navier-Stokes nonlinearity a mode needs a partner in a different block, or two modes in the same block unite to excite a mode in a different block.

In this section we will analye the linear interactions, *i.e.*, the coupling of the disturbance to the laminar background flow, and hence study every $[m|\beta]$ block on its own.

Stokes modes, being the eigenfunctions of the linearized Navier-Stokes equation for $Re = 0$, have the invaluable advantage of mutual orthogonality. But they lack appropriateness to the flow at sizable values of $Re$. It takes, for example, at least 15 Stokes modes per block to approximate a flow at $Re \approx 2000$. If one tries to get on with less, linear instabilities arise merely because the representation gets too bad although the flow actually is stable. Hence reducing the number of Stokes modes generates a system of differential equations wanting even structural similarity with real pipe turbulence.

Hagen modes, on the other hand, are defined as eigenfunctions of the Navier-Stokes equation linearized about the laminar Hagen-Poiseuille flow for every desirable value of $Re$. But, because this linear operator is nonnormal, they are not mutually orthogonal, even become almost degenerate (*i.e.*, nearly parallel) for increasing $Re$ and thus wreck numerical stability when the solution of the full Navier-Stokes equation is expanded in their terms. Moreover it is not the best idea to interpret the full Navier-Stokes solution in the Hagen mode representation. Namely, as shown in [1] Figures 26 and 27, the peculiarities of pipe turbulence then appear as minute differences of huge expansion coefficients.

Best seems an expansion in terms of a new set of modes which we call the *providers* and *consumers*. Their qualitative definition given in Section 1 is quantified here by a computational prescription: in a given space of flows we first construct an orthonormal set of functions $\mathbf{q}_\nu(\mathbf{r})$ and then follow the evolution of the disturbances $\mathbf{u}_\nu(\mathbf{r},t)$ originating from the $\mathbf{q}_\nu(\mathbf{r})$ by the linearized Navier-Stokes equation

$$L\mathbf{u}_\nu(\mathbf{r},t) = \partial_t \mathbf{u}_\nu(\mathbf{r},t) \quad \text{with } \mathbf{u}_\nu(\mathbf{r},0) = \mathbf{q}_\nu(\mathbf{r}).$$

$$L\mathbf{u} := -(\mathbf{U}_{\rm HP}\nabla)\mathbf{u} - (\mathbf{u}\nabla)\mathbf{U}_{\rm HP} - \nabla p - Re^{-1}\nabla\times\nabla\times\mathbf{u} \tag{1}$$

defines the linear operator with the basic Hagen-Poiseuille flow $\mathbf{U}_{\rm HP}$ and the pressure $p$. The Reynolds number $Re$ is defined in terms of the laminar profile's center velocity and the pipe's radius. To respect incompressibility of the flow, we solve (1) as vorticity equation. Energy and quality of the disturbance are defined by

$$\begin{aligned} E_\nu(t) &:= \frac{1}{2}\int_{\rm (pipe)} \mathbf{u}_\nu(\mathbf{r},t)^2 {\rm d}\tau, \\ Q_\nu(t) &:= E_\nu(t)/E_\nu(0) \quad \text{with} \\ & t = t_{{\rm max},\nu} \text{ or} \\ & t = \sqrt{Re}. \end{aligned} \tag{2}$$

If $Q_\nu(t)$ gets greater than one for $t > 0$, we call $\mathbf{q}_\nu(\mathbf{r})$ a provider and specify its quality by $\max_t Q_\nu(t)$; the corresponding time be $t_{{\rm max},\nu}$. However, all other functions, *i.e.*, the consumers, have $t_{{\rm max},\nu} = 0$ and $Q_\nu(0) = 1$. Therefore $Q_\nu(t_{{\rm max},\nu})$ wipes away all differences between the consumers. If these differences matter, we use $Q_\nu(\sqrt{Re})$ as a measure of the quality of the $\nu$th mode. $t = \sqrt{Re}$ was chosen since an estimate yields $t_{\rm max} \propto \sqrt{Re}$ for the providers at a given Reynolds number, see equation (60) in [1].

Practically the functions $\mathbf{q}_\nu(\mathbf{r})$ are constructed as columns of a unitarian matrix. First, we put the Hagen functions $\mathbf{h}_\nu(\mathbf{r})$ defined as the eigenfunctions of $L$

$$L\mathbf{h}_\nu(\mathbf{r}) = \mathbf{h}_\nu(\mathbf{r})\lambda_\nu \tag{3}$$

as columns into a matrix $H$ and, second, execute a $QR$ decomposition:

$$\begin{aligned} H = QR \quad &\text{with} \quad Q^{-1} = Q^\dagger \quad \text{and} \\ R = \{R_{ij} | R_{ij} = 0 \text{ for } i > j\}. & \end{aligned} \tag{4}$$

$Q$ is the afore-mentioned unitarian matrix. Devoting $Q$ as its symbol is a sacrosanct custom in linear algebra; $Q$ should not be confused with the qualities $Q_\nu(t)$. However, as $R$ is a right matrix, with nonzero elements only in its right upper half, the $QR$ decomposition can be construed as providing an orthogonalization: the primary vectors are put in as the columns of $H$, while the orthonormalized vectors come out as the columns of $Q$.

In pure mathematics one would prefer the Gram-Schmidt orthogonalization, but numerically the Gram-Schmidt method is not stable. Thus we accomplish the $QR$ decomposition by Householder's algorithm [8–11], which is stable. The resulting orthogonal vectors are, apart from factors of phase, unique.

The interpretation of the $QR$-decomposition is simplified by the following theorems. They are nothing than special extracts from Schur's reduction of an arbitrary square matrix to triangular shape [12], given here only to emphasize certain points that are important for our work.

### Theorem I

If the eigenvalue problem is defined by $LH = H\Lambda$ and $H = QR$, with $Q$ as unitarian and $R$ as right matrices, then $\tilde{L} := Q^\dagger L Q$ is a right matrix too.

*Proof*: from $LH = H\Lambda$ it follows $Q^\dagger L Q Q^\dagger H = Q^\dagger H \Lambda$. Hence $\tilde{L}R = R\Lambda$ or $\tilde{L} = R\Lambda R^{-1}$. Now, since $R$ is a right matrix, the inverse $R^{-1}$ is right as well. $\Lambda$ is just the diagonal matrix with the eigenvalues $\lambda_\nu$, hence a special right

$$\tilde{h}_{\mu\nu} = \begin{cases} 0, & \text{if } \mu = N, N-1, \dots, \nu+1; \\ 1, & \text{if } \mu = \nu; \\ \sum_{\kappa=\mu+1}^{\nu} \tilde{L}_{\mu\kappa}\tilde{h}_{\kappa\nu}/(\tilde{L}_{\nu\nu} - \tilde{L}_{\mu\mu}), & \text{if } \mu = \nu-1, \nu-2, \dots, 1. \end{cases}$$

**Table 1.** The matrix $\tilde{L} := Q^\dagger L Q$ of linear interactions for the 8-mode system in the block [+1|0.5] at $Re = 2000$. The matrix is based on the backward sequence defined in (5) with $N = 8$. The asteriks signal that this matrix element is bigger than the absolute value of the diagonal element in the same column.

| 1 | 2 | 3 | 4 | 5 | 6 | 7 | 8 | |
|---|---|---|---|---|---|---|---|---|
| −0.13 | 6e−2 | 9e−2 | 2e−2 | 2e−1 | 6e−2 | 7e−2* | 7e−2* | 1 |
| 0 | −0.12 | 1e−1 | 9e−2 | 3e−2 | 5e−2 | 2e−1* | 5e−2* | 2 |
| 0 | 0 | −0.12 | 7e−2 | 6e−2 | 1e−1* | 3e−1* | 1e−1* | 3 |
| 0 | 0 | 0 | −0.10 | 2e−2 | 6e−2 | 2e−1* | 2e−2 | 4 |
| 0 | 0 | 0 | 0 | −0.08 | 6e−2 | 1e−1* | 2e−1* | 5 |
| 0 | 0 | 0 | 0 | 0 | −0.08 | 1e−1* | 2e−1* | 6 |
| 0 | 0 | 0 | 0 | 0 | 0 | −0.06 | 3e−2 | 7 |
| 0 | 0 | 0 | 0 | 0 | 0 | 0 | −0.04 | 8 |

matrix. And a product of right matrices is again right. *q.e.d.*

Theorem I makes the realistic linear interaction operators $\tilde{L}$ directly comparable to the analytical toys that where created to make the peculiarities of pipe turbulence comprehensible [1, Section 4.2], [2], [5, Section 5], [7].

An example as in Table 1 exhibits the essentials. At first it appears puzzling because $\tilde{L} = \{\tilde{L}_{\mu\nu}|\mu, \nu = 1, \dots, 8\}$ is a complex matrix, whereas in the table only real numbers are given. This is the solution: the sub- and superdiagonal elements $\tilde{L}_{\mu\nu}, \mu \neq \nu$ are represented by their moduli $|\tilde{L}_{\mu\nu}|$. But in the diagonal there appear the real parts $\Re\tilde{L}_{\mu\mu}$ which are also the real parts of the eigenvalues of $\tilde{L}$, describing by their negative sign the decay of the Hagen functions, see Theorem II below.

The meaning of this format clears up when the linearized equations of motion $d_t a_\mu(t) = \sum_{\nu=1}^{N} \tilde{L}_{\mu\nu} a_\nu(t)$ with amplitudes $a_\mu(t)$ are considered. We can set $a_\mu(0) = \delta_{\mu\lambda}$ and estimate what the other amplitudes $a_\mu(t), \mu \neq \lambda$ do for $t > 0$. Namely, in first order the maximum size of those amplitudes is proportial to $|\tilde{L}_{\mu\lambda}|$ times the lifetime of the initially dominant $a_\lambda(t)$, which is $-1/\Re\tilde{L}_{\lambda\lambda}$. Hence comparing the superdiagonal elements with the numbers in the diagonal we can guess whether an amplitude $a_\mu(t)$ with a smaller value of its index $\mu < \lambda$ gets stronger than its pusher $a_\lambda(0)$. To make this visible, the matrix elements, which are bigger than the absolute value of the diagonal element in the same column, are distinguished by asterisks.

Table 1 suggests: providers appear for $\lambda = 8$ and $\lambda = 7$ with up to 6 asterisks and ratios $-|\tilde{L}_{\mu\lambda}|/\Re\tilde{L}_{\lambda\lambda}$ as high as 5. $\lambda = 6$ still has 1 asterisk, but the respective ratio is barely bigger than 1; hence $\mathbf{q}_6$ is at most a weak provider. All this is in keeping with Figure 4, which will be discussed later in more detail.

Moreover, the table exhibits that the providers $\mathbf{q}_8$ and $\mathbf{q}_7$ cause significantly different quality spectra. $\mathbf{q}_8$ is a poor provider of $\mathbf{q}_7$ and $\mathbf{q}_4$, whereas $\mathbf{q}_4$ is a favorite product of $\mathbf{q}_7$. To know this is valuable when one scrutinizes a solution of the nonlinear equations and wants to discriminate if a current amplification was caused by the providers $\mathbf{q}_7$ or $\mathbf{q}_8$.

Since $\tilde{L}$ is a right matrix and since it comprises all linear interactions, energy can flow only from higher to lower label value $q$-modes when the nonlinearities are suspended. Consequently the highest q-mode, here $\lambda = 8$, can be fed exclusively using the nonlinear manger. To some extent this is even true for $\lambda = 7$ because it is nourished but poorly by the linear interaction with $\lambda = 8$.

### Theorem II

The diagonal of the matrix $\tilde{L} = Q^\dagger L Q = \{\tilde{L}_{\mu\nu}|\mu, \nu = 1, \dots, n\}$ is occupied with the eigenvalues of $L$: $\tilde{L}_{\nu\nu} = \lambda_\nu$

*Proof*: one can verify this by direct calculation since the eigenvectors are given by

*see equation above*

$\tilde{h}_{\mu\nu}$ denotes the $\mu$th component of the eigenvector that belongs to the eigenvalue $\tilde{L}_{\nu\nu}$. Moreover $\tilde{L}$ emerges from $L$ by a similarity transform which cannot change the eigenvalues, thus $\tilde{L}_{\nu\nu} = \lambda_\nu$. *q.e.d.*

Theorem II warrants that the QR algorithm cannot import linear instabilities. So in (4) we can cancel Hagen functions whenever they appear to be less important and thus reduce the number of $q$-modes to be taken into account. With any other orthogonal system we cannot guarantee this. For example, reducing the number of Stokes functions below a certain limit depending on

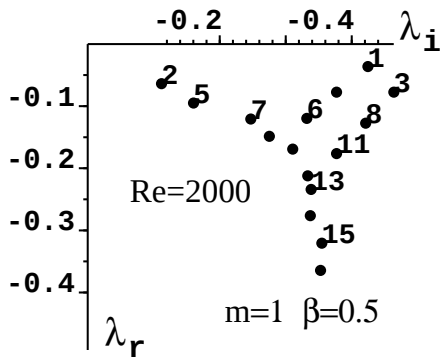


**Fig. 1.** The eigenvalues $\lambda_r + i\lambda_i$ of the linearized Navier-Stokes equation (1) are sorted according to increasing damping $-\lambda_r$. So eigenvalues 1 to 13 figure the "three-fingered swear hand", while the higher eigenvalues form the "arm", belonging to the deeply-damped modes. One of the central tasks of this study is to show that the powerhouse of pipe turbulence is built with the eigenfunctions belonging to the swear hand.

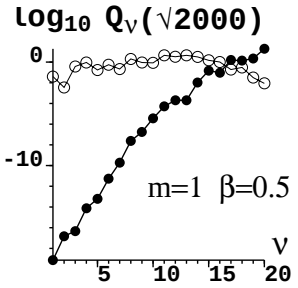


**Fig. 2.** The qualities of the **q**-modes from the forward (open) and the backward (closed symbols) sequence of the Hagen modes $\mathbf{h}_\nu$. $Q_\nu(t_{\max,\nu})$ was replaced by $Q_\nu(\sqrt{Re})$ to exhibit the differences between the consumers. $\nu$ numbers the modes; there is no symbol for the kinematic viscosity in this paper.

the Reynolds number induces linear instabilities that have nothing whatsoever to do with the physical problem. For the same reason a construction of modes based on singular value decomposition is suitable only if it is equivalent with our simpler prescription.

The sequence of orthogonalization, in other words, the sequence of the columns in $H$ influences the structure of the columns in $Q$. This is of utmost importance if the number of modes is to be reduced. Namely only the modes, which come last in the orthogonalization, can be omitted.

The following procedure produces the best results. We order the Hagen functions according to their dissipation, *i.e.*, first comes $\mathbf{h}_1(\mathbf{r})$ with the largest real part of its eigenvalue, *i.e.*, the smallest damping, confer with Figure 1. To construct an $N$-dimensional basis we consider the *backward sequence*

$$H := \{\mathbf{h}_N, \mathbf{h}_{N-1}, \dots, \mathbf{h}_1\} \tag{5}$$

and execute $QR$ decomposition. Then, in $Q$, the consumers fill the left columns (with the small values of the labels), whereas the providers are found in the rightmost columns (larger values of the labels). In most cases the functions are ordered with increasing quality corresponding to increasing value of the label.

An example is given in Figure 2. When we execute $QR$ decomposition with 20 Hagen modes $\mathbf{h}_\nu$ stuffed into $H$ as columns, 20 $q$-modes $\mathbf{q}_\nu$ appear as columns in $Q$. The space spanned by the $\mathbf{q}_\nu$ is, of course, invariant under the ordering of the $\mathbf{h}_\nu$ in $H$, yet for the properties of the individual $\mathbf{q}_\nu$ the order matters much. To demonstrate the essentials, results of the forward sequence $\mathbf{h}_1, \mathbf{h}_2, \dots, \mathbf{h}_{20}$ (open circles) are contrasted with those of the backward sequence (5) $\mathbf{h}_{20}, \mathbf{h}_{19}, \dots, \mathbf{h}_1$ (full circles). Equation (1) was solved, and $Q_\nu(\sqrt{Re})$ taken as a measure of the quality, see equation (2). In the case of the backward sequence the $\mathbf{q}_\nu$ are sorted according to increasing qualities, with the most powerful providers at big ordinals $\nu$. This is not so for the forward sequence.

To understand why the backward sequence is advantageous, consider the *forward sequence*

$$H := \{\mathbf{h}_1, \mathbf{h}_2, \dots, \mathbf{h}_N\}.$$

$QR = H$ means in its first line $\mathbf{q}_1 R_{11} = \mathbf{h}_1$ so that the first column of $Q$ and that of $H$ are identical up to a normalization. The second line $\mathbf{q}_1 R_{12} + \mathbf{q}_2 R_{22} = \mathbf{h}_2$ shows that the part of $\mathbf{h}_2$, which is parallel to $\mathbf{h}_1$, is covered by $\mathbf{q}_1$. $\mathbf{q}_2$ is needed only to deal with the orthogonal remainder of $\mathbf{h}_2$. In the last line $\sum_{\nu=1}^{N} \mathbf{q}_\nu R_{\nu N} = \mathbf{h}_N$, thus $\mathbf{q}_N$ appears as that column in $Q$ which is orthogonal to the first $N-1$ columns of $H$. In the sense discussed in Chapter 1 it therefore contains the coefficients of the most misfit function. Nevertheless $\mathbf{q}_N$ does not represent the best provider since it consists mostly of $\mathbf{h}_N$ and other strongly damped Hagen modes. For a good provider, orthogonality to most eigenfunctions must come with small damping. Exactly this is achieved by the backward sequence.

What happens if the number of Hagen functions and hence of q-modes is systematically reduced? To answer this, the sequences

| | |
|---|---|
| $\mathbf{h}_{20}, \mathbf{h}_{19}, \dots$ | $\mathbf{h}_1$ |
| $\mathbf{h}_{16}, \mathbf{h}_{15}, \dots$ | $\mathbf{h}_1, \mathbf{h}_{17}, \mathbf{h}_{18}, \mathbf{h}_{19}, \mathbf{h}_{20}$ |
| $\mathbf{h}_{13}, \mathbf{h}_{12}, \dots$ | $\mathbf{h}_1, \mathbf{h}_{14}, \mathbf{h}_{15}, \mathbf{h}_{16}, \mathbf{h}_{17}, \mathbf{h}_{18}, \mathbf{h}_{19}, \mathbf{h}_{20}$ |
| $\mathbf{h}_{12}, \mathbf{h}_{11}, \dots$ | $\mathbf{h}_1, \mathbf{h}_{13}, \mathbf{h}_{14}, \mathbf{h}_{15}, \mathbf{h}_{16}, \mathbf{h}_{17}, \mathbf{h}_{18}, \mathbf{h}_{19}, \mathbf{h}_{20}$ |
| $\mathbf{h}_{11}, \mathbf{h}_{10}, \dots$ | $\mathbf{h}_1, \mathbf{h}_{12}, \mathbf{h}_{13}, \mathbf{h}_{14}, \mathbf{h}_{15}, \mathbf{h}_{16}, \mathbf{h}_{17}, \mathbf{h}_{18}, \mathbf{h}_{19}, \mathbf{h}_{20}$ |

were processed by $QR$, and the qualities $Q_\nu(t_{\max,\nu})$ were computed solving the linearized Navier-Stokes equation (1). It must not be forgotten that, according to $QR$, only functions on the right-hand side can be omitted. For example, in the 11-sequence only the first 11 Hagen functions will be included in the solutions of the full, nonlinear Navier-Stokes equation which we will investigate in the next sections. The $q$-modes caused by the appendix $\mathbf{h}_{12}, \cdots, \mathbf{h}_{20}$ will be omitted there. Here, however, we have computed *all* 20 qualities in order to get a feeling what is lost if we forget about the Appendix. The results are shown in Figure 3. In the 20-sequence we discover four providers, with qualities clearly better than one. Reducing

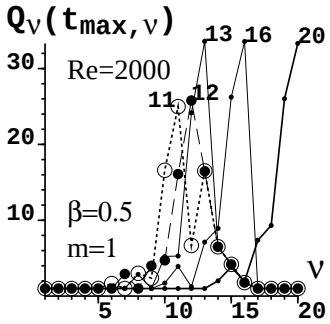


**Fig. 3.** The qualities of the **q**-modes for various sequences with $N = 11$, 12, 13, 16, or 20 modes. Here we used the measure of quality defined by $Q_\nu(t_{\max,\nu})$ with an individual time $t_{\max,\nu}$ for every mode. It is more precise for the providers.

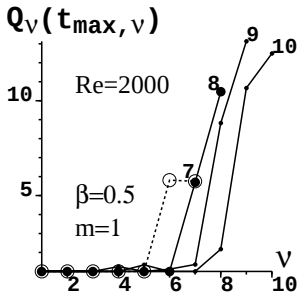


**Fig. 4.** Similar to Figure 3, this picture displays the qualities of the 7, 8, 9, 10-mode systems.

the number of included Hagen functions to 13 only shifts the quality spectrum to the left. The four providers are still included. The most powerful provider, in particular, does not diminish its quality. But in the 12-sequence (fat dots connected by the dashed lines) the most powerful q-mode $\mathbf{q}_{12}$ lost part of its quality to $\mathbf{q}_{13}$, which is assigned for later omission. Compare this with the situation of the eigenvalues in Figure 1. Quality gets really bad for the 11-sequence and, of course, for sequences with less modes. For the 11-sequence (big open circles connected by the dotted lines), only two good providers are included, *viz.* $\mathbf{q}_{11}$ and $\mathbf{q}_{10}$. The quality prevails now in $q$-modes that are to be omitted.

Further deterioration shows up in Figure 4. Down from the count $N = 8$ there are at most two providers. The 9-sequence plays a somewhat special role as it produces a provider that is better than the best in $N = 10$.

With decreasing number of $q$-modes we expect our representation of the Navier-Stokes equation to lose its ability of describing pipe turbulence. However, where exactly this happens must be tried by solving the full nonlinear system.

## 3 Closed communicating classes

The system of modes can by reduced in two ways: by diminishing the size of the blocks and by lessening the number of blocks. The second way will be pursued in this section.

Of the full Navier-Stokes equation

$$\partial_t \mathbf{U} = -(\mathbf{U}\nabla)\mathbf{U} - \nabla P - Re^{-1}\ \nabla\times\nabla\times\mathbf{U}, \qquad (6)$$

any mode expansion, if its elements are just proportional to $\mathrm{e}^{\mathrm{i}m\varphi}\,\mathrm{e}^{\mathrm{i}\beta z}$, evinces the selection rules for the nonlinear interaction

$$m_\kappa + m_\lambda = m_\mu, \quad \beta_\kappa + \beta_\lambda = \beta_\mu. \qquad (7)$$

Here $\kappa$ and $\lambda$ are the indices of the modes in the nonlinear interaction, while $\mu$ characterizes a mode behind the partial time derivative, to which the interaction contributes. In other words, $\kappa$ and $\lambda$ describe input blocks which excite modes in the output block $\mu$: $[m_\kappa|\beta_\kappa]*[m_\lambda|\beta_\lambda] \to [m_\mu|\beta_\mu]$.

In reference [1] checks with 9 or even 10 blocks were carried out to ensure the reliability of the results. Mostly, however, the following 6-block system was engaged:

$$[-1|1.0],\ [0|1.0],\ [+1|1.0],\ [-1|0.5],\ [0|0.5],\ [+1|0.5]. \qquad (8)$$

The numbers in the parentheses represent the values of $[m|\beta]$. To secure the reality of the solution, 6 further blocks with negative $\beta$ have to be added, but these are coupled to the already considered ones by complex conjugacy, *i.e.*,

$$[-m|-\beta] \equiv [m|\beta]. \qquad (9)$$

The combination of equations (7) through (9) results in the following multiplication table

$$\begin{array}{llll}
[0|1.0]*[-1|0.5]\to[+1|0.5] & & [-1|1.0]*[-1|0.5]\to[0|0.5] & \\
[0|1.0]*[0|0.5]\to[0|0.5] & & [-1|1.0]*[0|0.5]\to[-1|0.5] & \\
[0|1.0]*[+1|0.5]\to[-1|0.5] & & & \\
[+1|1.0]*[0|0.5]\to[+1|0.5] & & [-1|0.5]*[0|0.5]\to[-1|1.0] & \\
[+1|1.0]*[+1|0.5]\to[0|0.5] & & [-1|0.5]*[+1|0.5]\to[0|1.0] & \\
[0|0.5]*[0|0.5]\to[0|1.0] & & & \\
[0|0.5]*[+1|0.5]\to[+1|1.0]\,. & & & 
\end{array} \qquad (10)$$

This table, equation (10), exhibits two subsets of *closed* communicating classes contained in (8):

$$[0|1.0]\,,\quad [0|0.5] \qquad (11)$$

and

$$[0|1.0]\,,\quad [-1|0.5]\,,\quad [+1|0.5]\,. \qquad (12)$$

(11) is of no use for the description of pipe turbulence as it consists only of axisymmetric modes that cannot draw energy from the basic flow. But (12) has the salient properties of the much larger systems, in particular it describes the double threshold, see Figure 5. Yet it is more vigorous: it allows for turbulence already at Reynolds numbers as low as $Re \approx 1000$, and the energy of the turbulent disturbance $E_{\mathrm{dis}}(t)$ becomes larger than in the 6-block system. One can understand this from the data presented in Figure 13 of [1]: the modes of the block $[+1|0.5]$ deliver stronger energy amplification than those of block $[+1|1.0]$, let alone those of $[+1|0.25]$ or with $m = 2$ or $m = 3$.

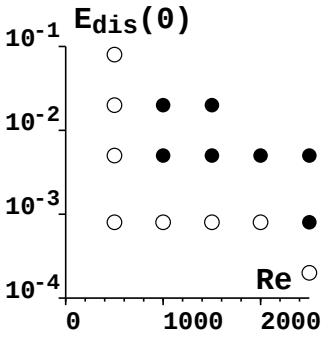


**Fig. 5.** The double threshold for the 3-block system (12) with 20 Stokes modes per block. A circle indicates a quick return to laminarity, whilst a fat dot represents a turbulent run. The initial conditions were set as $a_{m=0,\beta=-1.0,\nu=2}(0) = a_{m=-1,\beta=-0.5,\nu=2}(0) = a_0$ with the $a_{\dots}(t)$ as amplitudes of the Stokes modes. $a_0$ is a real number tuned to yield the initial energy $E_{\rm dis}(0)$. All other amplitudes were 0 at the beginning. These computations were done with the Stokes functions because we do not need the **q**-modes to find the closed communicating classes. The two ways of reduction, *viz.* lessening the count of blocks and diminishing their size, are independent. However, it was checked that computations with 20 **q**-modes produce the same diagram and, apart from rounding errors, even the same runs (at least as long as the time intervals are limited).

In other words: extensive numerical examination has shown that blocks with $[m = 1|\beta \approx 0.5]$ give the most powerful energy amplification attainable in pipe flow. The block [0|1.0], on the other hand, sponges on energy. We are tempted to discard it, too, yet it is indispensible for the nonlinear interaction: without [0|1.0] we cannot form a closed communicating class.

In the same wise as the 3-block systems are closed communicating sub-classes in 6-block systems, the 6-systems themselves are just closed communicating classes in the even larger 9- or 10-systems. In this sense the 3-block systems are the smallest ones to describe salient properties of pipe turbulence.

The idea of a closed communicating class stems from the theory of Markov chains, see *e.g.* [13].

## 4 Powerhouse and consumption: minimum mode number

We now have the tools to systematically reduce the degrees of freedom. We take the vorticity of the nonlinear Navier-Stokes equation (6), use $N$ **q**-modes by backward sequences (5), sort out the 3 blocks (12) and transform the partial differential equation (6) into $3 \times N$ ordinary differential equations for complex amplitudes by Galerkin's familiar procedure.

Some representative solutions are recorded in Figure 6 by their energy of disturbance $E_{\rm dis}(t)$. At least two peculiarities are remarkable.

The initial decrease of $E_{\rm dis}(t)$ comes much more from the energetic redistribution than from the loss by viscosity. *E.g.* in the $3 \times 20$–mode system, the 2 initial modes excite the residual 58 modes until there is the right nonlinear interaction to prepare linear energy amplification; in the $3 \times 7$–mode system only 19 sleeping modes must be roused. So it is not by accident that $E_{\rm dis}$ tumbles faster in the $3 \times 20$–mode system than in its $3 \times 7$–mode comrade. This is one observation to underline the importance of phase-space investigations.

After the initial drop of $E_{\rm dis}(t)$ the $N$-dependence of the time development exhibits the features predicted in Figures 3 and 4 for the (linear) qualities $Q_\nu$. Just quick returns to laminarity, but no turbulent ups and downs are observed in the $3 \times 7$–mode system and smaller ones. The $3 \times 8$–mode system produces transients typically fading at $t \approx 300$, yet with turbulent interims. Most remarkable are the huge fluctuations in the $3 \times 13$–mode system that hustle to the infinities for $t > 100$. The $3 \times 20$–mode system, however, looks again reasonable.

The difference between the $3 \times 20$– and the $3 \times 13$–mode systems is easily understood with the help of Figure 3: in both systems there are 4 powerful providers granting about the same amplifications. But the consumers are more numerous in the $3 \times 20$–mode system, and they consume much more energy since they comprise the deeply-damped Hagen modes $\mathbf{h}_{14}, \cdots, \mathbf{h}_{20}$, compare Figure 1.

One can think of this as being due to a balance between the *powerhouse* and the *consumption*. The powerhouse would be the set of all providers, while all other degrees of freedom would constitute the consumption. The $3 \times 13$–mode system is thus the most overpowered engine we can have at $Re = 2000$: it has the complete powerhouse, whereas the consumption is minimized. When the count of modes drops below $N = 13$, the powerhouse is gradually destroyed until it cannot supply the disturbance with sufficient energy. This limit shows up at $N = 8$ and is definitely crossed at $N = 7$.

Therefore a system with $3 \times 8$ complex degrees of freedom seems to provide the minimum description of pipe turbulence at $Re = 2000$. Nevertheless we cannot exclude the possibility of lowering this number. Namely, we considered an equal number of modes in all three blocks. But the block [0|1.0] is structurally different from the blocks $[-1|0.5]$ and $[+1|0.5]$, so [0|1.0] might do with less modes.

Having understood the ideas of the powerhouse and the consumption, one may even tame the $3 \times 13$–mode system. All one has to do is to take the sequence $\mathbf{h}_{13}, \mathbf{h}_{12}, \dots, \mathbf{h}_1$ and to replace some of the weakly-damped (lower label values) Hagen modes by their deeply-damped brethren.

## 5 Refueling the powerhouse

What has been discussed over and over again was how a provider pushes the consumers thus causing amplification of the disturbance. But what takes care of the provider when it is finished, *i.e.*, when its energy is exhausted? Clearly, only the nonlinearity! The first kind of nonlinearity (a mode cooperates with a partner in a different block) becomes effective when at least one mode in the

**Table 2.** Actions from the interactions between blocks [0|1.0] and [+1|0.5]. The block symbols are abbreviated as $0\backslash+1$ to appear in the upper-left corner of the table. On output the actions are total; everything that appears in the block [−1|0.5] contributes additively to them. The computations were done with the 3-block system and 8 modes per block. Therefore this table is closely related to Figures 4 and 6, and to Table 1. Of all numbers at most two leading figures are given because the actions will be used for estimates only.

| $0\backslash+1$ | 1 | 2 | 3 | 4 | 5 | 6 | 7 | 8 |
|---|---|---|---|---|---|---|---|---|
| 1 | 5300 | 950 | 20000 | 2000 | 120000 | 7200 | 2500 | 130000 |
| 2 | 900 | 46 | 660 | 210 | 11000 | 6200 | 860 | 6200 |
| 3 | 7100 | 81 | 13000 | 1700 | 61000 | 15000 | 2300 | 36000 |
| 4 | 720 | 9 | 230 | 20 | 9400 | 2100 | 690 | 3100 |
| 5 | 7 | 640 | 210 | 11000 | 310 | 290 | 3500 | 410 |
| 6 | 130 | 540 | 220 | 420 | 1200 | 78 | 610 | 650 |
| 7 | 2800 | 2200 | 25000 | 1200 | 100000 | 130000 | 1900 | 140000 |
| 8 | 860 | 200 | 790 | 160 | 440 | 2700 | 290 | 2400 |

**Table 3.** Akin to Table 2. Here the actions generated by the q-modes in the blocks [+1|0.5] and [−1|0.5] are presented. The actions comprise everything roused in block [0|1.0].

| $+1\backslash-1$ | 1 | 2 | 3 | 4 | 5 | 6 | 7 | 8 |
|---|---|---|---|---|---|---|---|---|
| 1 | 58 | 15 | 150 | 8 | 860 | 370 | 560 | 1400 |
| 2 | 10 | 15 | 52 | 44 | 94 | 27 | 460 | 120 |
| 3 | 123 | 53 | 330 | 34 | 1000 | 1200 | 1700 | 780 |
| 4 | 12 | 23 | 30 | 300 | 61 | 150 | 790 | 130 |
| 5 | 890 | 130 | 1200 | 34 | 6200 | 6900 | 6200 | 96000 |
| 6 | 430 | 28 | 960 | 70 | 6300 | 9200 | 3500 | 3500 |
| 7 | 1000 | 890 | 2500 | 1100 | 5100 | 5600 | 14000 | 34000 |
| 8 | 1400 | 99 | 680 | 91 | 89000 | 2900 | 17000 | 230000 |

block [0|1.0] and one in [+1|0.5] ally to rouse a provider in [−1|0.5]. Yet this is not sufficient: the modes in [0|1.0] must be kept alive by the second kind of nonlinear interaction (two modes in the same block unite to excite a mode in a different block), *viz.* between blocks [−1|0.5] and [1|0.5].

To find the thread how these two kinds of nonlinearities work, we proceed as follows: for the initial conditions we endow only two **q**-modes in two different blocks with non-zero amplitudes. Namely, two modes excited in two different blocks is minimum for the initiation of nonlinear interactions. With this peculiar initial condition the full, nonlinear differential equations are solved and the amplitudes in the third block are recorded. Based on these amplitudes, the computation of the actions

$$S^{M\mu}_{K\kappa,\Lambda\lambda} = \int_0^{t_{\max}} a^2_{M\mu}(t)\mathrm{d}t \Big/ \left(a^2_{K\kappa}(0)a^2_{\Lambda\lambda}(0)\right) \qquad (13)$$

is straightforward. The indices $K, \Lambda, M = +1, 0, -1$ are cyclical block labels. They are meant to discriminate blocks, with +1 as shorthand for [+1|0.5], 0 for [0|1.0] etc. The lower case indices $\kappa, \lambda, \mu = 1, \ldots, N$ denote mode labels. The quotient in (13) is to be construed as a limiting value for $a^2_{K\kappa}(0) \to 0$ and $a^2_{\Lambda\lambda}(0) \to 0$. In other words, we choose the initial amplitudes of the modes $K\kappa$ and $\Lambda\lambda$ small enough to keep nonlinear feedback between these modes themselves negligible since we want to see just what blocks $K$ and $\Lambda$ do to $M$. Also subsequent interactions *e.g.* between $K$ and $M$ or $\Lambda$ and $M$ would destroy clearness.

Therefore, in the limit considered here, the amplitude $a_{M\mu}(t)$ in the third block starts at 0 for $t = 0$, $a^2_{M\mu}(t)$ then reaches a maximum at $t_{\max}$, and finally the amplitude approaches again 0. So we might extend the integration to infinity, but don't do it to save computational time. Of course, here $t_{\max}$ depends on all 6 labels, but in practice it is always of the order $\sqrt{Re}$.

For simplicity it sometimes is better not to specify the individual modes on output. We then prefer to compute the sum of all amplitudes squared in the third block, *i.e.*, twice the energy in this block, and omit the mode index $\mu$ to write the sum as $a^2_M(t)$.

Using the action $\int_0^{t_{\max}} a^2_M(t)\mathrm{d}t$ instead of the energy $a^2_M(t)/2$ has the advantage of magnifying differences. For the sustenance of turbulence, the linear processes, which can start again their effectiveness when a nonlinear interaction happened to rouse a provider, are important. Although we want to expose the nonlinear interaction which creates such a provider, we can make that more visible by letting it grow under subsequent linear amplification.

**Table 4.** Actions created by blocks [+1|0.5] and [−1|0.5], similar to Table 3. But the actions here are specified to measure only the excitation of the 1st q-mode in block [0|1.0]. Notice the small size of these actions. One should expect them to contribute 1/8 to the total actions in Table 3 if one relies in statistical arguments.

| $+1\backslash -1$ | 1 | 2 | 3 | 4 | 5 | 6 | 7 | 8 |
|---|---|---|---|---|---|---|---|---|
| 1 | 0.004 | 0.005 | 1 | 0.08 | 4 | 10 | 0.3 | 5 |
| 2 | 0.010 | 0.02 | 0.9 | 0.04 | 1 | 9 | 0.5 | 5 |
| 3 | 0.7 | 0.2 | 0.6 | 0.2 | 27 | 43 | 19 | 140 |
| 4 | 0.2 | 0.3 | 0.02 | 0.4 | 28 | 30 | 3 | 99 |
| 5 | 2 | 1 | 22 | 4 | 4 | 56 | 92 | 2800 |
| 6 | 10 | 2 | 28 | 4 | 110 | 3 | 63 | 720 |
| 7 | 1 | 0.5 | 71 | 8 | 170 | 430 | 8 | 240 |
| 8 | 4 | 3 | 230 | 5 | 2500 | 560 | 340 | 190 |

But these secondary linear processes take time and are thus better observed in the action.

And these are the lessons to be learnt from the Tables 2, 3, and 4, which comprise our results concerning the strategy of the Navier-Stokes interaction to rouse providers and thus to sustain turbulence.

Start with Table 2: in the interaction between blocks [0|1.0] and [+1|0.5] the strongest actions are produced by modes $\mathbf{q}_1$ and $\mathbf{q}_5$, $\mathbf{q}_1$ and $\mathbf{q}_8$, $\mathbf{q}_7$ and $\mathbf{q}_5$, $\mathbf{q}_7$ and $\mathbf{q}_6$, $\mathbf{q}_7$ and $\mathbf{q}_8$. The 1-5 interaction is especially valuable because it works without the providers, which are discernible by mode numbers 7 and 8.

A glimpse at Table 3 reveals: in the interaction between blocks [+1|0.5] and [−1|0.5] strongest actions arise with modes $\mathbf{q}_5$ and $\mathbf{q}_8$, $\mathbf{q}_8$ and $\mathbf{q}_5$, $\mathbf{q}_8$ and $\mathbf{q}_8$. This type of nonlinearity cannot thrive without a provider.

Tables 2 and 3 contain total actions only. Table 4, by contrast, presents actions specific for the viscously least damped mode $\mathbf{q}_1$ in [0|1.0]. For we know from Table 2 that $\mathbf{q}_1$ plays a prominent role for the permanence of turbulence. We find in Table 4 that modes $\mathbf{q}_5$ and $\mathbf{q}_8$ or $\mathbf{q}_8$ and $\mathbf{q}_5$ in [+1|0.5] and [−1|0.5] push $\mathbf{q}_1$ in [0|1.0] best, in agreement with Table 3.

The conclusion is that as few as 5 modes might constitute a perpetuum mobile of pipe turbulence, *viz.* both $\mathbf{q}_5$ and $\mathbf{q}_8$ in [+1|0.5] and [−1|0.5], and $\mathbf{q}_1$ in [0|1.0], all other modes just featuring those beautiful turbulent ornaments. This is demonstrated in Figure 6, which offers the temporal development of the energy of a disturbance calculated with different sets of modes. Spectral analysis reveals that the 5-8-1-5-8 mechanism is indeed present in various regeneration phases. But there are also other growth cycles with different spectral dominances, *i.e.*, that mechanism is nothing but a special case to regenerate turbulence.

To demonstrate that the 5-8-1-5-8 mechanism works we look at Figure 7 which, together with the next figure (Fig. 8), displays the signature of this process. It shows an example how two consumers use the nonlinear interaction to rouse a provider, thus enabling amplification of the disturbance.

At $t = 0$ the energy is concentrated in two blocks [+1|0.5] and [0|1.0], and there it resides in two modes only: $\mathbf{q}_5$ and $\mathbf{q}_1$. Their output appears in the third block, *viz.*

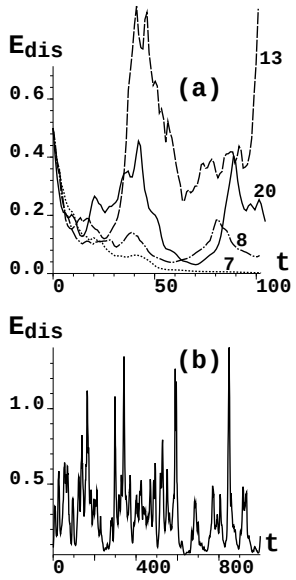


**Fig. 6.** (a) The energy $E_{\rm dis}(t)$ of the disturbance obtained from the 3-block systems with $N = 7$, 8, 13, and 20 modes per block. Always the same initial conditions were imposed, namely the least dissipating Hagen functions $\mathbf{h}_1$ in the blocks [+1|0.5] and [0|1.0]. For $\mathbf{h}_1$ is contained in all sequences, irrespective of $N$. The 7 and 8 mode systems do not have sufficient energy supply and decay. The 13 mode system is properly fed but the consumers, *i.e.*, modes with strong viscous damping, are not yet sufficiently included, thus the solution becomes diverging. The 20 mode system fluctuates irregularly. (b) Longer time solution (up to $t = 1000$) of the 3 block and 20 modes per block system, $Re = 2000$. This provides a characteristic example for the long lasting irregular fluctuations looking like chaos or turbulence.

[−1|0.5]. Nonlinear feedback, for instance between blocks [0|1.0] and [−1|0.5], is admitted but weak since the initial excitations were chosen to be small.

Within a block energy flows only downward due to the triangular shape of the linear interaction matrix $\tilde{L}$. An impressive example of this law can be seen in the block [0|1.0]; not even a morsel of intensity is spread to the

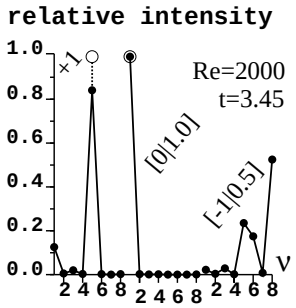


**Fig. 7.** The relative intensities of the nonlinear $3 \times 8$–mode system as they evolve within a finite time $t$. The initial values at $t = 0$ are indicated by the open circles. At $t = 3.45$ the distribution is represented by the full dots. The lines connect intensities belonging to the same block: $[+1|0.5]$, $[0|1.0]$ or $[-1|0.5]$, $+1$ being shorthand for $[+1|0.5]$. For all times the sum of intensities in every block is kept at unity; this is why these intensities are qualified as *relative*.

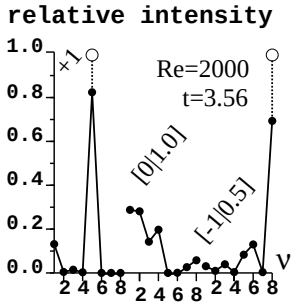


**Fig. 8.** The same kind of relative intensities as in Figure 7.

higher modes. By the same argument we know that $\mathbf{q}_8$ in $[-1|0.5]$ is exclusively pushed by the *nonlinear* interaction. However, as a consequence of this excitation of $\mathbf{q}_8$, which is the best provider in the system, the lower modes in $[-1|0.5]$ are largely stirred by the *linearity*. Notice the dents in the intensity spectrum at $\nu = 4$ and $\nu = 7$, and compare this with the corresponding 4 and 7 dips in the last column of Table 1.

Modes with azimuthal symmetry, in particular those in block $[0|1.0]$, are indispensable for pipe turbulence, yet, as it was shown in [1], have no means of linear amplification. Their survival relies entirely on the nonlinearity. How this happens is shown in Figure 8. The initial conditions, *i.e.*, the modes $\mathbf{q}_5$ in block $[+1|0.5]$ and $\mathbf{q}_8$ in $[-1|0.5]$, were selected to provoke an especially strong excitation of $\mathbf{q}_1$ in $[0|1.0]$, confer with Table 4.

The intensity spectrum in the block $[0|1.0]$ is atypic. With most other initial conditions the even modes at $\nu = 2, 6, 8$ come out much stronger whereas $\mathbf{q}_1$ is suppressed. Nevertheless we have seen that $\mathbf{q}_1$ in $[0|1.0]$ is important for rousing a provider in $[+1|0.5]$ or $[-1|0.5]$. So the process shown here plays a key role for the sustenance of pipe turbulence. $\mathbf{q}_1$ in $[0|1.0]$ is a toroidal mode with strong components of velocity perpendicular to the pipe's axis.

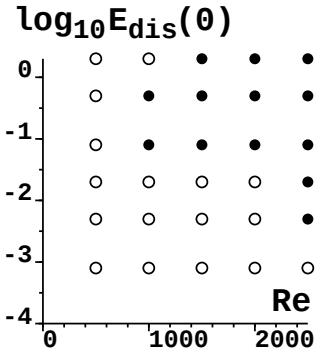


**Fig. 9.** The double threshold for the onset of turbulence of the $3 \times 8$–mode system depending on the Reynolds number $Re$ and on the initial strength of the disturbance $E_{\rm dis}(t = 0)$. The latter is a kinetic energy formed as in (2), however, its time dependence (which decides whether being laminar or turbulent) is calculated now with the full nonlinear system. Apart from a multiplier, which determines the size of $E_{\rm dis}(0)$, the initial conditions are the same as for the trajectory shown in Figure 6, *viz.* just the least-damped Hagen modes were excited. Full dots indicate that from this initial condition a trajectory evolves which exhibits fluctuations as displayed in Figure 6 for $0 \leq t \leq 100$. Trajectories that decay before $t = 100$ are considered as laminar solutions. They are represented by open circles.

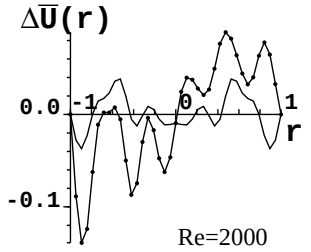


**Fig. 10.** Time-averaged velocity profiles as functions of the radial distance $r$. Just differences $\Delta\overline{U}(r) = \overline{U}(r) - \overline{U}_{\rm HP}(r)$ between the actual, full and the laminar Hagen-Poiseuille profiles are plotted. $r$ takes negative values, too, to depict what happens across a complete pipe diameter ranging from $-1 \leq x, y \leq 1$. It is the line with the dots which exhibits $\Delta\overline{U}(r)$. The fat line displays the symmetrized profile $\{\Delta\overline{U}(r) + \Delta\overline{U}(-r)\}/2$. The Reynolds number is $Re = 2000$, the number of modes is 48.

Comparing Figure 8 with Figure 7 you might notice the similarity of the spectra in blocks $[+1|0.5]$ and $[-1|0.5]$, in particular the dents at $\nu = 4$ and $\nu = 7$ of $[-1|0.5]$. The similarity is due to the fact that most redistribution in these blocks is caused by linear processes.

## 6 Turbulence-like features of the solutions

As was said already in the introduction, we may compare properties obtained from the $3 \times N$ solutions of the Navier-Stokes equation with measured quantities of real pipe flow in order to justify the notion "turbulent" for our small $N$

flows. We have already considered the irregular fluctuations as one characteristic though qualitative feature of turbulent flows. We now present two more properties, the double threshold (Fig. 9) and the flattening of the pipe's velocity profile (Fig. 10), both calculated with the $3 \times 8$–mode system.

As we selected a special class of initial disturbances, we cannot claim to produce a double threshold, which can be compared quantitatively with measured ones, although we always find the same qualitative structures. Yet for all Reynolds numbers shown in Figure 9, we took pains to minimize the number $N(Re)$ of modes that still produce turbulent-looking solutions. So $N(2500) = 10$, $N(2000) = 8$, $N(1500) = 9$, $N(1000) = 8$. We do not find long-lasting fluctuations for $Re = 500$, however, the system generating most powerful but short and thus non-turbulent fluctuations has $N(500) = 10$. In other words, we strengthen the powerhouse and keep the consumption as low as possible. Therefore it is not surprising to find turbulent solutions at $Re$ as low as 1000.

Long experience with similar systems has shown us that the open circle at $Re = 1000$ and $E_{\rm dis}(0) = 2$ is not accidental. It is as if all these systems had, at low Re, only a limited provision of fluctuations which is sooner worn out when the initial disturbance is gross.

As for the velocity profile we cannot expect sizeable modifications of the Hagen-Poiseuille profile at $Re = 2000$. No wonder the experimentalists present deformed profiles usually at Reynolds numbers not less than 4000. We nevertheless take the risk to show the velocity profiles at $Re = 2000$ even for our reduced mode number solutions and find results, Figure 10, which are compatible with the measurements at higher Reynolds numbers.

The data was computed with the $3 \times 8$ system, and the same initial conditions were imposed as for the trajectory shown in Figure 6. At $Re = 2000$ most turbulent transients do not live long. For the time averages displayed here only times $t < 251.7$ were available. Moreover, we discarded the first short time interval to get rid of the initial dispersion (recognizable in Fig. 6) reducing the time range used for averaging to $5.2 < t < 251.7$.

Figure 10 indicates something that might be novel and to be confirmed by experiments. Because the effects are small, we have plotted the results as differences $\Delta\overline{U}(r)$.

Concentrate first on the fat line. $\Delta\overline{U}(r)$ was symmetrized to improve the statistics. Disregarding the large fluctuations, the symmetrized profile looks almost as expected. We observe a depression at the center $-0.4 < r < 0.4$ and enhancements closer to the pipe wall. Yet the negative values of $\Delta\overline{U}(r)$ at $r \approx \pm 0.9$ look awkward. The temptation to declare them as random blunders must be forsaken since many other trajectories exhibit similar features.

The reason behind these near-wall depressions shows up when the nonsymmetrized profile is considered. Instead of the central depression we see a retardation at $r \approx -0.9$ and an acceleration for $r > 0$. At the transition to turbulence in diffusers, this asymmetric flow pattern is known as *stall* and was discovered experimentally, see Figure 175 in [15]. Based on the results from the tiny $3 \times 8$ system we suggest now that similar stalls or blackflows guide the onset of turbulence in pipes.

One should check, of course, this backflow by computations with more modes, and one must explain why these blackflows are not observed at higher Reynolds numbers. For this the results are already at hand. Figure 3 of [1] shows a similar backflow at $Re = 3000$ computed with $6 \times 20$ modes. The only essential difference between our findings here and those in [1] is that at $Re = 3000$ the turbulent transients live much longer. The blackflow itself is not stable. It appears at some position of the pipe's wall, then resolves and reappears somewhere else. So in long-time averages the backflow phenomena are smeared out.

## 7 Summary: Tools and applications

The systematic simplification of the equations describing pipe flow is the main content of this paper. Four applications were derived from it.

The first result is 90% or even higher savings of computer resources. The research on the physical mechanisms of the onset of turbulence in a pipe is possible on a PC already.

Second, as the reduction stopped at 48 degrees of freedom, we have now another argument for the fundamental difference between turbulence in shear flows and in the Rayleigh-Bénard system where a reduction to three degrees of freedom at onset was possible. The present result puts additional evidence to the previous finding [14] that a low-dimensional chaotic attractor in pipe turbulence does not seem to exist.

Third, the reduction is more than just a diminution of counts. It separates the energy providers from the consumers. This gave insights into the working of the Navier-Stokes equation: if the community of providers is strengthened, the ODEs produce run-away solutions. If the consumers prevail, fast relaxation to zero is unavoidable. Only the balance between powerhouse and consumption enables turbulent-looking solutions.

Fourth, by a special example it was shown how the powerhouse is refueled by the nonlinear terms in the Navier-Stokes equation. We made efforts to identify the most important nonlinear mechanism. Nevertheless we must concede that our favorite mechanism is only one among many others.

Two tools were used for the reduction: the **q**-modes and the closed communicating classes, consisting of blocks which are characterized by symmetry labels.

A small closed communicating class simplifies the nonlinear interactions. The method is applicable only if the basic flow exhibits symmetries that categorize the modes in blocks. For pipe flow, three of these blocks can be put together to form a closed communicating class which is sufficient for a crude description of turbulence.

The **q**-modes are obtained from the eigenfunctions of the Hagen-Poiseuille linearized Navier-Stokes equation by

plain orthogonalization employing the $QR$-decomposition. Surprising is just the backward sequence (5) as it produces **q**-modes which are ordered according to their quality (2).

We acknowledge support of this wook by the German-Israeli Foundation (GIF).

## References

1. L. Boberg, U. Brosa, Z. Naturforsch. A **43**, 697 (1988).
2. J.S. Baggett., L.N. Trefethen., Phys. Fluids **9**, 1043 (1997).
3. A. Schmiegel, B. Eckhardt, Phys. Rev. Lett. **79**, 5250 (1997); see also B. Eckhardt, K. Marzinzik, A. Schmiegel, in *A Perspective Look at Nonlinear Media*, Edited by J. Parisi, S.C. Mueller, W. Zimmermann, Lecture Notes in Physics **503**, pp. 327–338. (Springer, Berlin, 1998).
4. B. Eckhardt, A. Mersmann, Transition to turbulence in a shear flow, preprint (1997).
5. S. Grossmann, Phys. Bl. **51**, 641 (1995).
6. T. Gebhardt, S. Grossmann, Z. Phys. B **90**, 475 (1993).
7. T. Gebhardt, S. Grossmann, Phys. Rev. E **50**, 3705 (1994).
8. A.S. Householder, *The Theory of Matrices in Numerical Analysis* (Blaisdell, New York, 1964).
9. J. Stoer, *Einführung in die Numerische Mathematik I* (Springer, Berlin, Heidelberg, New York, 1979).
10. G.H. Golub, Ch.F. van Loan, *Matrix Computations*, 2nd edn. (Johns Hopkins University Press, Baltimore, 1989).
11. W.H. Press, B.P. Flannery, S.A. Teukolsky, W.T. Vetterling, *Numerical Recipes in C* (University Press Cambridge, 1988).
12. I. Schur, Math. Ann. **66**, 488 (1909).
13. E. Parzen, *Stochastic Processes* (Holden-Day, San Francisco, 1962).
14. U. Brosa, J. Stat. Phys. **55**, 1303 (1989) and references therein.
15. M. van Dyke, *An Album of Fluid Motion* (The Parabolic Press, Stanford, 1982).
16. S. Grossmann, Rev. Mod. Phys. (to appear, 1999).